Biophysical Journal Volume 96 May 2009 4085–4098

Penetration Depth of Surfactant Peptide KL_4 into Membranes Is Determined by Fatty Acid Saturation

Vijay C. Antharam,[‡§] Douglas W. Elliott,[‡§] Frank D. Mills,[‡§] R. Suzanne Farver,[‡§] Edward Sternin,[†] and Joanna R. Long[‡§*]

[†]Department of Physics, Brock University, St. Catharines, Ontario, Canada; and [‡]Department of Biochemistry and Molecular Biology, and [§]McKnight Brain Institute, University of Florida, Gainesville, Florida

ABSTRACT KL_4 is a 21-residue functional peptide mimic of lung surfactant protein B, an essential protein for lowering surface tension in the alveoli. Its ability to modify lipid properties and restore lung compliance was investigated with circular dichroism, differential scanning calorimetry, and solid-state NMR spectroscopy. KL_4 binds fluid lamellar phase PC/PG lipid membranes and forms an amphipathic helix that alters lipid organization and acyl chain dynamics. The binding and helicity of KL_4 is dependent on the level of monounsaturation in the fatty acid chains. At physiologic temperatures, KL_4 is more peripheral and dynamic in fluid phase POPC/POPG MLVs but is deeply inserted into fluid phase DPPC/POPG vesicles, resulting in immobilization of the peptide. Substantial increases in the acyl chain order are observed in DPPC/POPG lipid vesicles with increasing levels of KL_4, and POPC/POPG lipid vesicles show small decreases in the acyl chain order parameters on addition of KL_4. Additionally, a clear effect of KL_4 on the orientation of the fluid phase PG headgroups is observed, with similar changes in both lipid environments. Near the phase transition temperature of the DPPC/POPG lipid mixtures, which is just below the physiologic temperature of lung surfactant, KL_4 causes phase separation with the DPPC remaining in a gel phase and the POPG partitioned between gel and fluid phases. The ability of KL_4 to differentially partition into lipid lamellae containing varying levels of monounsaturation and subsequent changes in curvature strain suggest a mechanism for peptide-mediated lipid organization and trafficking within the dynamic lung environment.

INTRODUCTION

Lung surfactant is a lipid-rich substance containing key proteins that minimizes surface tension in the alveoli and provides a barrier against disease (1,2). Lung surfactant undergoes a cycle of lipid adsorption and resorption at the alveolar air-fluid interface. Lipid polymorphisms that change the geometry and arrangement of lipid headgroups have been postulated to be critical for this process not only in the lung, but also in other membrane-membrane mediated events (3,4). The lipid constitution in mammalian lung surfactant is heterogeneous but is dominated by zwitterionic PC (70–80%) and 10–20% anionic PG and PI (5); ~50% of the PC lipids and almost all of the anionic lipids in lung surfactant are monounsaturated. Levels of the lipids are relatively conserved in the lungs of vertebrates (6), with the preponderance of DPPC being particularly striking. The stability of DPPC-enriched monolayers at air-water interfaces is of particular relevance in the lung environment. However, the lipid composition of lung surfactant is not sufficient to explain its unique properties. Critical to its function are the lung surfactant proteins, which are present at relatively low levels (7). In particular, SP-B, which accounts for 0.7–1.0% of the dry weight of lung surfactant, or <0.2 mol % relative to the lipids, is required for proper lung function (8). Disruption of the SP-B gene in mice confers embryonic lethality (9) and mutations cause respiratory failure (10,11). Inadequate protein levels are a leading cause of RDS in premature infants (12).

A multitude of roles for SP-B in surface tension minimization, intracellular surfactant trafficking, and respiratory dynamics in general have been proposed and experimentally established (13). Current therapies for RDS primarily rely on administration of lung surfactant isolates from animal sources to replenish SP-B (14,15). The native form of SP-B is a highly hydrophobic, 78–81 residue protein that functions as a homodimer and contains seven disulfide bridges (16–18). The hydrophobicity and disulfide bridges within SP-B make purification or heterologous expression of the protein in large quantities untenable. Structurally, SP-B has been postulated to be primarily helical based on CD and FTIR studies of the isolated protein in a phospholipid environment (19,20). However, more detailed structural studies of SP-B

Submitted September 9, 2008, and accepted for publication December 23, 2008.

*Correspondence: jrlong@mbi.ufl.edu

Abbreviations used: PC, phosphatidylcholines; CD, circular dichroism; PG, phosphatidylglycerol; PI, phosphatidylinisotol; CPMAS, cross-polarization with magic angle spinning; CSA, chemical shift anisotropy; DPPC, 1,2-dipalmitoyl-*sn*-glycero-3-phosphocholine; DPPC-d_{62}, 1,2-d_{62}-dipalmitoyl-*sn*-glycero-3-phosphocholine; DSC, differential scanning calorimetry; FTIR, Fourier transform infrared; H_{II}, inverted hexagonal phase; LUV, large unilamellar vesicle; $L_{\alpha\alpha}$, fluid lamellar phase; L_{β}, gel lamellar phase; MLV, multilamellar vesicle; NMR, nuclear magnetic resonance; P/L, peptide/lipid molar ratio; POPC, 1-palmitoyl-2-oleoyl-*sn*-glycero-3-phosphatidylcholine; POPC-d_{31}, 1-d_{31}-palmitoyl-2-oleoyl-*sn*-glycero-3-phosphatidylcholine; POPG 1-palmitoyl-2-oleoyl-*sn*-glycero-3-phosphatidylglycerol; POPG-d_{31}, 1-d_{31}-palmitoyl-2-oleoyl-*sn*-glycero-3-phosphatidylglycerol; RDS, respiratory distress syndrome; SP-B, surfactant protein B; ssNMR, solid-state nuclear magnetic resonance; TFE, trifluoroethanol; TM, transmembrane.

Editor: Lukas K. Tamm.

0006-3495/09/05/4085/14 $2.00

doi: 10.1016/j.bpj.2008.12.3966

have been precluded by its hydrophobicity and consequent problematic isolation and purification (21–23). Synthetic, peptide-based lung surfactant replacements designed to replicate the properties of SP-B have received noticeable attention (24) as the use of synthetic analogs would remove the immunologic risks associated with animal-derived surfactant and allow for greater restorative consistency. Peptide mimics that rely on the presumption of amphipathic helicity in SP-B have been pursued both clinically and as model systems for understanding the structure and dynamics of the protein and lipids that impart the unique physical properties of lung surfactant. Understanding how peptide analogs of SP-B alter lipid properties could lead to the design of SP-B mimetics with enhanced biophysical properties and therapeutic lifetimes. For example, oligo N-substituted glycines (phenylethyl, 2-butyl, or 4-aminobutyl substituents attached to the nitrogen of glycine), or peptoids, have been designed to mimic the helicity of SP-B and have shown potential (25).

KL_4, or sinapultide, was designed based on amino acid residues 59–80 of SP-B and has particularly strong surface tension reducing properties (26). The primary amino acid sequence of KL_4 is a repeating pattern of four hydrophobic leucines separated by hydrophilic lysines: KLLLLKLLLLK LLLLKLLLLK. KL_4 has shown promise as a replacement for therapies that rely on exogenous SP-B (27–31). KL_4-based surfactant therapy relies on a formulation of the peptide with DPPC, POPG, and a spreading agent, palmitic acid. Molecular-level information on how synthetic peptides can modulate surface tension in alveolar compartments is limited; however, lucinactant, the clinical name for KL_4 in a lipid formulation, has been approved as an agent for treatment of RDS because of its efficacy. In vitro assays as well as animal studies have shown the ability of KL_4 to lower surface tension in different lipid systems (26,32). In clinical studies, administration of lucinactant to very premature infants was noticeably more effective in treating RDS than other commercially available formulations (33). KL_4 improves respiratory status and was found to prevent the appearance of diffuse, granular radiopacity seen in chest radiographs typical of RDS and meconium aspiration syndrome (27,28). A recent antimicrobial function of KL_4 was also suggested, in line with recent reports concerning the antibacterial properties of SP-B (34,35). However, the biophysical properties of KL_4 and their relation to alleviating RDS remain the focal point of current investigations, particularly in regard to its structure and organization in lipid environments.

Artificial lung surfactant formulations simplify the problem of studying the underlying biophysical aspects of lung surfactant function against the complicated, heterogeneous background that exists in vivo. Of particular interest is that KL_4 retains many of the macroscopic properties of SP-B even though it bears little resemblance to the biologically produced protein other than a similarity in charge distribution to the C-terminus. With an understanding of the properties of KL_4, nonnatural peptide analogs of SP-B that exploit the protein's helical and amphipathic qualities could be made to extend or enhance artificial lung surfactant therapies. Thus, understanding how KL_4 affects the molecular and biophysical properties of lipids is of particular relevance for the treatment of various forms of RDS. The use of calorimetry and CD in combination with ssNMR can provide unique insight into KL_4-induced changes in lipid phase properties. In this study, static ^2H and ^{31}P NMR, MAS ^{13}C NMR, CD, and DSC were employed to investigate the properties of mixtures of KL_4 with 4:1 DPPC/POPG and 3:1 POPC/POPG lipid vesicles. The former lipid composition was selected to mirror the lipid composition of several lung surfactant studies and lucinactant. The latter composition is similar to formulations used in numerous studies of amphipathic membrane-active peptides (36–38) and allows direct comparison of the physical properties of KL_4 with other biologically active peptides. Lipid phases of these compositions can also be found in localized areas of the alveoli during the surfactant cycle.

MATERIALS AND METHODS

Synthesis of KL_4

KL_4 (KLLLLKLLLLKLLLLKLLLLK) was synthesized via automated solid-phase peptide synthesis on a Wang resin (ABI 430, ICBR, UF). The peptide was cleaved from the resin with 90% TFA/5% triisopropyl-silane/5% water and ether precipitated. The crude product was purified by reverse-phase high-performance liquid chromatography using an acetonitrile/water gradient, and purity was verified by mass spectrometry. Dried peptide was weighed and dissolved in methanol to a stock concentration of ~1 mM, and aliquots were analyzed by amino acid analysis (Molecular Structure Facility, University of California, Davis, CA) for a more accurate determination of concentration.

Preparation of peptide/lipid samples

POPC, DPPC, POPG, POPC-d_{31}, DPPC-d_{62}, and POPG-d_{31} were purchased as chloroform solutions (Avanti Polar Lipids, Alabaster, AL) and concentrations were verified by phosphate analysis (39) (Bioassay Systems, Hayward, CA). The lipids were mixed at a molar ratio of 4:1 DPPC/POPG and 3:1 POPC/POPG in chloroform and aliquoted. For samples containing peptide, a methanol solution of KL_4 was added to lipid solutions with final protein/lipid (P/L) molar ratios ranging from $<$1:1000 to $>$1:50. The samples were dried under a stream of nitrogen with the sample temperature maintained at 42–50°C in a water bath. The resulting films were suspended in cyclohexane, flash-frozen, and lyophilized overnight to remove residual solvent.

CD experiments

For CD experiments, 3 mg of peptide-lipid powder were solubilized in 1 mL 10 mM HEPES buffer, pH 7.4, with 140 mM NaCl to achieve a concentration of 40 μM KL_4 with 4 mM lipids. Samples were placed in a 50°C water bath to facilitate solubilization accompanied by three to five freeze-thaw cycles with vortexing to achieve equilibration. Peptide-lipid MLVs were extruded through 100 nm filters (Avanti Polar Lipids, Alabaster, AL) 15–25 times above the T_m of the lipids to form LUVs just before CD analysis. CD experiments were performed on an Aviv model 215 (Aviv, Lakewood, NJ) at 45°C using a 195–260 nm wavelength range, a 1 nm step size,

and averaging of 10–25 scans. A control spectrum of 40 μM KL_4 in TFE was also collected. Background contributions from the buffer and LUVs were removed by subtracting appropriate controls.

DSC experiments

For DSC experiments, 2 mg of peptide-lipid powder was solubilized in 1 mL of 5 mM HEPES buffer, pH 7.4, with 140 mM NaCl, 1 mM EDTA, and, in some cases, 5 mM $CaCl_2$ to achieve a 3 mM lipid concentration. Samples were placed in a 50°C water bath to facilitate solubilization accompanied by three to five freeze-thaw cycles with vortexing to achieve equilibration. Peptide-lipid MLVs were extruded through 100 nm filters (Avanti Polar Lipids, Alabaster, AL) 15–25 times at 45°C to form LUVs and degassed just before DSC. DSC experiments (MicroCal, LLC, Northampton, MA) were conducted over a range of 10–70°C at a scan rate of 1°C/min and run in triplicate.

^{31}P and ^{2}H NMR experiments

For each static ssNMR sample, 20–30 mg of peptide-lipid powder was placed in a 5 mm diameter NMR tube with 200–300 μL of buffer containing 5 mM HEPES pH 7.4, 140 mM NaCl, and 1 mM EDTA in ^{2}H depleted water (Cambridge Isotopes, Andover, MA). Samples were made using 4:1 DPPC-d_{62}/POPG, 4:1 DPPC/POPG-d_{31}, 3:1 POPC-d_{31}/POPG, 3:1 POPC/POPG-d_{31}, DPPC-d_{62}, POPC-d_{31}, or POPG-d_{31} lipid preparations. Some NMR samples contained 5 mM $CaCl_2$; however, we saw no significant difference in NMR line shapes between samples with or without Ca^{2+}. NMR samples were subjected to three to five freeze-thaw cycles with gentle vortexing to form MLVs before data collection. ^{31}P NMR data were collected on a 600 MHz Avance system (Bruker, Billerica, MA) using a standard 5 mm broadband probe. Proton decoupling (25 kHz) was employed during acquisition to remove dipolar couplings. Spectra were acquired at 34°C, 39°C, and 44°C with 1024–2048 scans and a 5 s recycle delay between scans to minimize radiofrequency sample heating. ^{2}H NMR data were collected on a 500 MHz Bruker Avance system using a standard 5 mm broadband probe and quad echo sequence (90°-τ-90°-τ-acq with $\tau = 30$ μs) with a B_1 field of 40 kHz. Spectra were acquired at 34°C, 39°C, and 44°C for all samples with 1024 or 2048 scans and a 0.5 s recycle delay between scans. To monitor the phase transitions of the DPPC/POPG mixtures, for some samples spectra were also collected over a range of 30–44°C in 2° increments.

DePaking analysis of NMR data was accomplished using previously published algorithms that simultaneously dePake and determine macroscopic ordering for partially aligned lipid spectra using Tikhonov regularization (40). ^{31}P NMR spectra were referenced to phosphate buffer before dePaking, and dePaked spectra were quantitated by fitting the resulting two peaks with Lorentzian line shapes. Assignments of ^{2}H resonances were made based on published values (41,42).

MAS NMR analysis

For each sample, 40 mg of lipid containing KL_4 ^{13}C′-enriched at positions L9 and L10 at a P/L ratio of 1:33 or 1:100 were hydrated in 1 mL of buffer containing 10 mM HEPES pH 7.4, 140 mM NaCl, and 1 mM EDTA. Samples were subjected to 3–5 freeze-thaw cycles with gentle vortexing to form MLVs before pelleting the lipids by centrifugation. The pellets were packed directly into MAS rotors and NMR data were collected at temperatures of ~−5°C, 25°C, and 40°C. NMR samples contained ~20 mg of the lipid-peptide mixture.

MAS experiments were performed on a 500 MHz DRX system (Bruker, Billerica, MA) using a doubly tuned 4 mm magic angle spinning probe (Doty Scientific, Columbia, SC). CPMAS experiments employed a ^{1}H 90° pulse width of 3.2 μs followed by a contact time of 2 ms and 100 kHz ^{1}H CW decoupling. A 25% ramp was applied on the ^{1}H channel during cross polarization. Spectra were acquired at a spinning speed of 5 kHz with a total of 512–2048 scans for each spectrum. The rotor speed was regulated to ±3 Hz for all MAS experiments, and each transient was collected with a sweep width of 50 kHz and 20 ms of acquisition (1024 points) with a recycle delay of 3 s between transients.

For the ^{1}H spin diffusion experiments (43), residual ^{13}C magnetization was abolished by four 90° pulses before excitation of ^{1}H magnetization. After a 90° pulse on the ^{1}H channel, a T_2 filter was applied for 10 rotor periods (2 ms) to dephase ^{1}H magnetization in any rigid molecules before the t_1 period for evolution of the ^{1}H magnetization. After the evolution period, the magnetization was stored along the z axis for 100–200 ms to allow ^{1}H spin diffusion before the magnetization was flipped back to the x-y plane with a 90° pulse. The ^{1}H magnetization was then transferred to neighboring ^{13}C spins by a short (0.5 ms) cross-polarization period followed by detection of the ^{13}C signal with 100 kHz ^{1}H CW decoupling. The 2D spectra were collected with 512 transients per t_1 point and 96 spectra were collected over the course of 19.2 ms in t_1 (a dwell time of one rotor period) using States-Haberkorn-Ruben phase-sensitive detection.

RESULTS

Secondary structure of KL_4 interacting with lipid bilayers

CD spectroscopy was utilized to investigate the conformation of KL_4 in the presence of unilamellar lipid vesicles. The effects of two lipid systems—a 4:1 DPPC/POPG lipid mixture and a 3:1 POPC/POPG lipid mixture—on peptide secondary structure were investigated. Fig. 1 shows the CD spectra obtained for KL_4 in these two environments. Spectra were collected at 45°C to ensure that both lipid systems were in the liquid lamellar phase. As a control, the CD spectrum of KL_4 in 50% TFE is shown for comparison. The CD spectra have features characteristic of helical secondary structure, as evidenced by minima at 206–208 and 222 nm. The spectra differ for the two lipid environments, and the spectrum for KL_4 interacting with 4:1 DPPC/POPG shows greater helicity than the spectrum for KL_4 interacting with 3:1 POPC/POPG lipids. Of interest, the samples containing DPPC/POPG LUVs have similar ellipticity to the peptide in TFE, with the minimum at

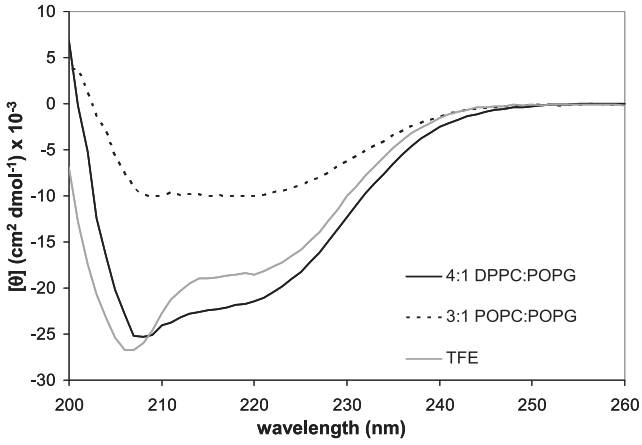

FIGURE 1 CD spectra at 45°C of KL_4 at a P/L molar ratio of 1:100 in 4:1 DPPC/POPG (*solid dark curve*), at a P/L molar ratio of 1:100 in 3:1 POPC/POPG (*dashed curve*) and in 50% TFE (*solid shade curve*). The final peptide concentration was 40 μM in all three samples.

206–208 significantly lower than the minimum at 222 nm. Similar spectra have been observed for peptides that were constrained to form π-helices in buffer (44). In a first attempt to understand the origins of the differences seen in the CD spectra, the data were fit with standard deconvolution software (45), resulting in secondary structure estimates of 40–45% α-helix, 40–45% random coil, and 10–20% β-sheet for KL_4 in POPC/POPG LUVs and >85% α-helix, <15% random coil, with negligible β-sheet for KL_4 in DPPC/POPG LUVs. However, the quality of the fits was poor, particularly for the sample containing DPPC/POPG LUVs, due to the nonstandard shape of the CD spectra relative to canonical α-helices, which have minima of similar depths at 222 and 208 nm, and to the lack of data below 200 nm, where light scattering from the lipids prevents signal measurement. Given that KL_4 does not form a typical amphipathic α-helix when projected on a helical wheel (Fig. 2 *A*), it is highly probable that the peptide forms helices that might vary in helical pitch or even hydrogen-bonding patterns. More amphipathic helical wheel projections for KL_4, which represent structures that KL_4 might adopt in lipid bilyers, along with their hydrophobic moment values, are shown for comparison (Fig. 2, *B* and *C*).

DSC suggests KL_4 decreases DPPC/POPG lipid miscibility

Shown in Fig. 3 are DSC thermograms for 4:1 DPPC/POPG LUVs containing varying levels of KL_4. Adding POPG to DPPC in a 1:4 ratio results in a lipid transition temperature below 37°C, >4° lower than the T_m for pure DPPC, due to the monounsaturated fatty acid group in POPG. Of note is the gradual shift of T_m to a higher temperature as KL_4 levels are increased. At 0.2 mol % peptide, a higher temperature shoulder appears in the phase transition. This shoulder grows with increasing levels of peptide until two peaks with T_m values of 37°C and 39°C are clearly seen at 1 mol % peptide. At 2 and 3 mol % peptide the higher temperature transition becomes dominant. This bifurcation in the phase transition suggests domain separation of the lipids, possibly due to electrostatic interactions between the cationic peptide and anionic POPG. This phase separation is striking given the low percentages of peptide, and is similar to behavior noted

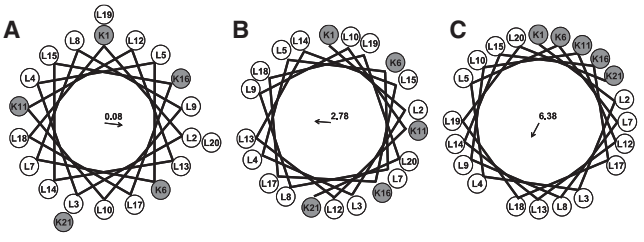

FIGURE 2 Helical wheel representations of KL_4 assuming (*A*) a canonical α-helix, (*B*) a helix with a pitch intermediate between α-helix and π-helix, and (*C*) a π-helix.

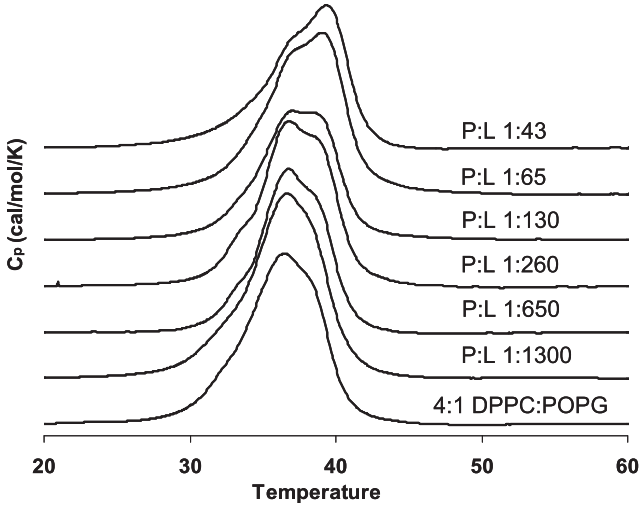

FIGURE 3 DSC scans for 4:1 DPPC/POPG LUVs with KL_4 at the indicated P/L ratios. The onset of phase separation is apparent at a P/L ratio of 1:260 and continues with increasing amounts of peptide.

previously for 3:1 DPPC/POPG MLVs (46). It also agrees with a previous observation of domain formation via Langmuir trough studies of KL_4 interacting with fluorescently labeled DPPC in a DPPC/POPG/PA system (47). This behavior may be important for the function of the peptide in vivo during the lipid resorption/adsorption cycle (13). However, from the DSC data it is not possible to determine whether the separate transitions are due to the formation of separate POPG-enriched and POPG-depleted DPPC lipid domains or to another physical phenomenon. In particular, leucine-rich TM peptides have been demonstrated to cause phase separation when interacting with DPPC. The two transitions observed in DSC traces are attributed to melting of bulk lipids and peptide-associated lipids (48). Given the high percentage of leucines in KL_4, close association of the peptide with lipid fatty acyl chains is expected. Other than a small increase at low concentrations of KL_4, no significant change in ΔH_{cal} was seen. DSC samples with 5 mM $CaCl_2$ showed a similar behavior, indicating that the effects of KL_4 on the L_β-to-L_α phase transition in this lipid system is not calcium-dependent.

Effect of KL_4 on lipid headgroup interactions

ssNMR was used to obtain a molecular-level view of how KL_4 interacts with phospholipids in the two bilayer systems. ^{31}P NMR spectra at 44°C for 3:1 POPC/POPG and 4:1 DPPC/POPG MLVs containing varying concentrations of KL_4 were collected and dePaked, allowing a clear determination of the individual, time-averaged CSAs of the PC and PG headgroups (Fig. 4). Because data were collected on a 600 MHz NMR spectrometer, macroscopic alignment of the vesicles occurred, as evidenced by the downfield features in the lamellar line shapes being lower in intensity than is typically seen for phospholipid dispersions at lower

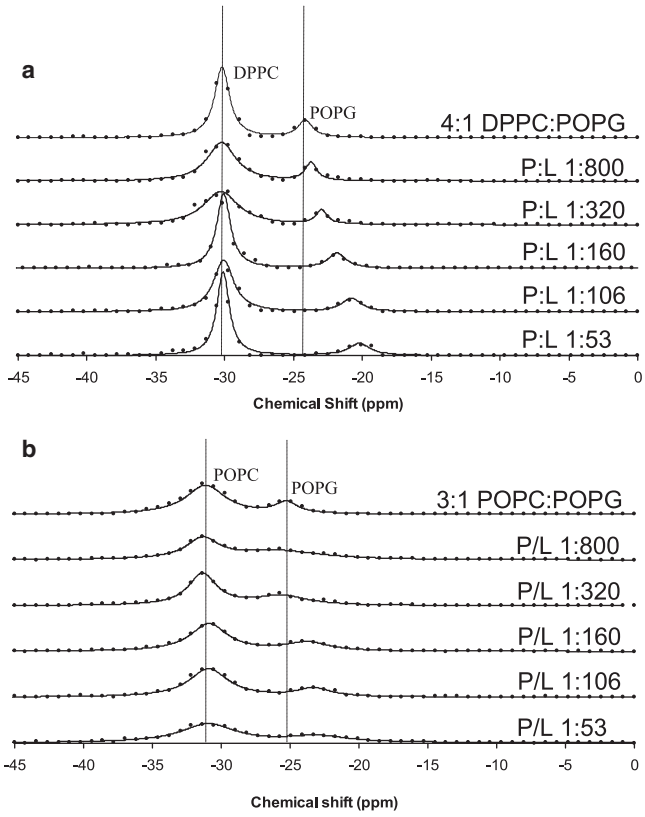

FIGURE 4 DePaked phosphorous NMR spectra of (*top*) 4:1 DPPC/POPG and (*bottom*) 3:1 POPC/POPG MLVs with KL_4 at the indicated P/L ratios with fits assuming Lorentzian line shapes.

magnetic fields (Supporting Material). As such, standard fitting of the chemical shift powder patterns was not possible. Instead, a dePaking algorithm that includes a Tikhonov regularization procedure for correcting for the macroscopic alignment was utilized (40). From this analysis it is possible to determine the spans of the CSA patterns and hence deduce the effects of KL_4 on the phospholipid headgroups. Differences in PG and PC headgroup orientations relative to the membrane normal lead to differences in their CSA values (49). With increasing levels of KL_4, the PC CSA was invariant, but the PG CSA lessened with increasing peptide levels. The decrease in the POPG CSA on addition of KL_4 was consistently seen in all lipid systems studied, regardless of which lipid was deuterated. To assess the underlying cause of the changes in POPG CSAs, ^{31}P NMR spectra were collected on individual lipids alone and with 1.5 mol % KL_4; the ^{31}P NMR spectra and their corresponding dePaked spectra are provided in the Supporting Material. Only small changes in individual lipid CSAs were seen on addition of KL_4. However, the CSA for POPG alone is significantly smaller than that observed for POPG in 4:1 DPPC/POPG or 3:1 POPC/POPG mixtures before the addition of KL_4. For the binary lipid mixtures containing higher concentrations of KL_4, the ^{31}P CSAs are more comparable to those of the neat lipids. Thus, KL_4 clearly affects the interactions of the PC and PG lipids, and possibly their miscibility. Table 1 shows CSA values for lipid mixtures and comparisons with individual lipids. These results indicate that when POPG interacts with PC headgroups, electrostatic interactions cause the PG headgroups to reorient, leading to a subsequent increase in their averaged CSA values. Addition of KL_4 disrupts this interaction, causing the PG CSAs to move toward values seen for POPG alone.

At low P/L ratios, lipid alignment along the static magnetic field is seen in spectra of lipid systems, as evidenced by disproportionately high perpendicular edges for the static powder patterns. Lipid alignment in high magnetic fields was observed previously (40,50,51) and is caused by the negative diamagnetic susceptibility inherent to phospholipids. In lipid bilayers, the cooperative alignment of the magnetic moments of individual lipid molecules leads to a large bulk magnetic susceptibility resulting in an overall macroscopic ordering of the sample within the magnetic field. Increasing amounts of KL_4 disrupt this alignment in a concentration-dependent manner, as evidenced by the gradual increase in the parallel edges of the ^{31}P NMR spectra. The reduction in alignment of the lipid lamellae on addition of KL_4 suggests that the peptide disrupts lipid-lipid interactions. The ability of peptides to affect lipid magnetic field alignment, particularly for amphipathic peptides, was previously noted (52–56). However, reports on the influence of amphipathic peptides on lipid alignment have been primarily anecdotal, and the diversity in lipid composition, peptide concentration, and experimental conditions used to date prohibit a systematic evaluation of how peptide sequences and lengths affect macroscopic lipid organization. Finally, for our systems, although the POPG CSA values decrease on addition of KL_4, the lipids clearly remain in a lamellar phase above the phase transition temperature.

TABLE 1 ^{31}P CSA values (in ppm) for 3:1 POPC/POPG and 4:1 DPPC/POPG with varying concentrations of KL_4 (peaks in the dePaked spectra had full widths at half-height of 1–5 ppm)

	4:1 DPPC/POPG		3:1 POPC/POPG	
mol % KL_4	DPPC	POPG	POPC	POPG
0	44.8	38.2	45.8	38.6
.06	46.0	37.6	46.0	38.5
.13	45.4	37.8	46.2	38.7
.2	44.8	37.4	44.0	38.4
.31	45.2	37.1	45.1	38.6
.63	45.8	36.2	45.3	37.3
.94	46.1	35.2	46.4	36.6
1.0	45.0	35.2	44.7	36.7
1.89	45.5	34.9	45.8	36.9
3.0	45.0	32.7	44.5	35.3
	Individual lipids			
	DPPC	POPG	POPC	
0	48.0	34.4	46.2	
1.5	44.6	34.7	47.3	

^{2}H NMR studies of DPPC/POPG lipid miscibility on addition of KL_4

To determine whether the domain formation observed in the DSC experiments was due to phase separation of the DPPC and POPG lipids, ^{2}H NMR spectra were collected over the temperature range of the phase transitions for samples that contained either deuterated DPPC or deuterated POPG (Fig. 5). A first-moment analysis of these data to determine the phase transition temperatures is provided in the Supporting Material. From these spectra, it is clear that in the 4:1 DPPC/POPG samples the lipids are fully miscible, with the DPPC and POPG melting at similar temperatures. The phase transition seen for deuterated DPPC is at a slightly *lower* temperature (midpoint of 30.7°C) than for deuterated POPG (31.1°C). This is partly because a larger percentage of the fatty acyl chains is deuterated (80% vs. 10%) (57), but it may also reflect slight differences in POPG content between the two samples since they were made from different lipid stock solutions. For the samples that do not contain KL_4, the spectra at intermediate melting temperatures are a superposition of gel phase and liquid phase spectra. Addition of KL_4 affects the phase transition temperature of both lipids in a similar manner, based on the first-moment analysis. However, in the POPG-d_{31} spectra a larger percentage of the dynamic lipid phase is evident, and in the DPPC-d_{62} spectra the dynamic phase is absent at lower temperatures, as can be seen by comparing spectra at 30°C and 32°C. The peptide also leads to an increase in temperature at which the lipids are completely melted (36°C vs. 40°C for deuterated DPPC; 38°C vs. 40°C for deuterated POPG), consistent with the DSC data. Attempts to determine the fractions of liquid phase and gel phase by spectral subtractions with samples containing differing percentages of KL_4 were unsuccessful due to variations in the lipid alignment and acyl chain order parameters. Thus, addition of KL_4 leads to some phase separation of the lipids at lower temperatures, with a significant fraction of POPG remaining in the gel phase. Above the phase transition temperature of the domain with the higher T_m, the peaks in the ^{2}H spectra coalesce to a single resonance for each position in the acyl chain, suggesting the absence of separate domains in the fluid phase or exchange between domains is fast on the NMR timescale.

Effects of KL_4 on lipid acyl chain dynamics

Further analysis of ^{2}H NMR spectra above the lipid phase transition temperatures allows determination of the effect of KL_4 on lipid acyl chain dynamics in the fluid phase, and provides insight into its partitioning depth into the bilayers. ^{2}H NMR spectra for 3:1 POPC-d_{31}/POPG and 4:1 DPPC-d_{62}/POPG MLVs at 44°C with varying levels of KL_4 were collected and dePaked (Fig. 6). For 3:1 POPC-d_{31}/POPG MLVs, only small decreases are seen in the ordering of the POPC *sn*-1 acyl chains on addition of KL_4. In contrast, addition of KL_4 to 4:1 DPPC-d_{62}/POPG MLVs increases the ordering of the DPPC acyl chains, particularly toward the middle of the bilayer. This suggests that either 1), KL_4 inserts deeply into the DPPC/POPG bilayers, restricting the motional freedom of the acyl chains; or 2), an electrostatic interaction of the peptide with the lipid headgroups occurs, resulting in a change in the lipid packing and headgroup conformation. However, the ^{31}P experiments described above establish that the phosphate moieties in the PC headgroups are unaffected by KL_4, ruling out the latter possibility.

Lipid acyl chain order parameters were determined by measuring the quadrupolar splitting ($\Delta\nu_Q$) for deuterium atoms at various positions along the acyl chain and determining their order parameters, S_{CD} (Eq. 1). The order parameters provide a measure of the average angular fluctuations around the bilayer normal at each acyl chain segment (58):

$$\Delta\nu_Q = \frac{3}{4}\frac{e^2qQ}{h}\left(3\cos^2\theta - 1\right)S_{\mathrm{CD}}. \qquad (1)$$

For saturated C-D bonds, the quadrupole coupling, $\frac{3}{4}\frac{e^2qQ}{h}$, is 167 kHz in the static limit (59). If the bilayers adopt random orientations with respect to the magnetic field, the resulting spectra of perdeuterated acyl chains are comprised of a superposition of axially symmetric powder patterns arising from each deuterated position. The intensities of these powder patterns follow the well-established distribution function $p(\theta) \propto \sin(\theta)$, where θ is the angle between the

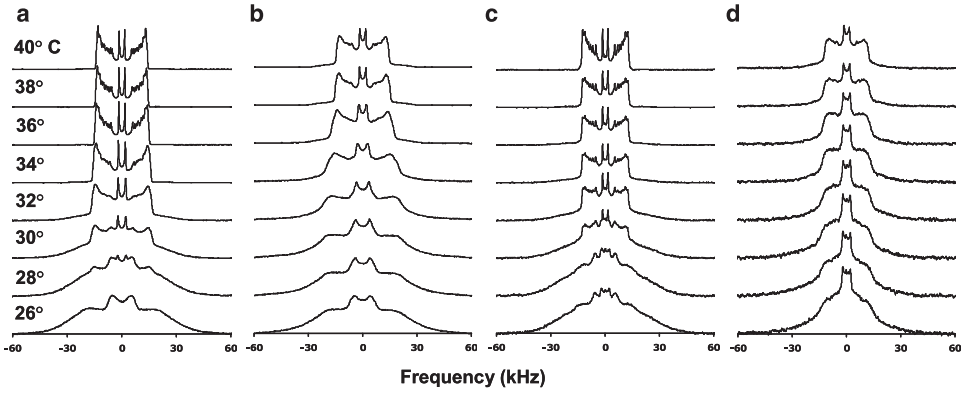

FIGURE 5 Deuterium NMR spectra as a function of temperature for (*a*) 4:1 DPPC-d_{62}/POPG MLVs, (*b*) 4:1 DPPC-d_{62}/POPG MLVs with KL_4 at a P/L molar ratio of 1:53, (*c*) 4:1 DPPC/POPG-d_{31} MLVs, and (*d*) 4:1 DPPC/POPG-d_{31} MLVs with KL_4 at a P/L molar ratio of 1:33.

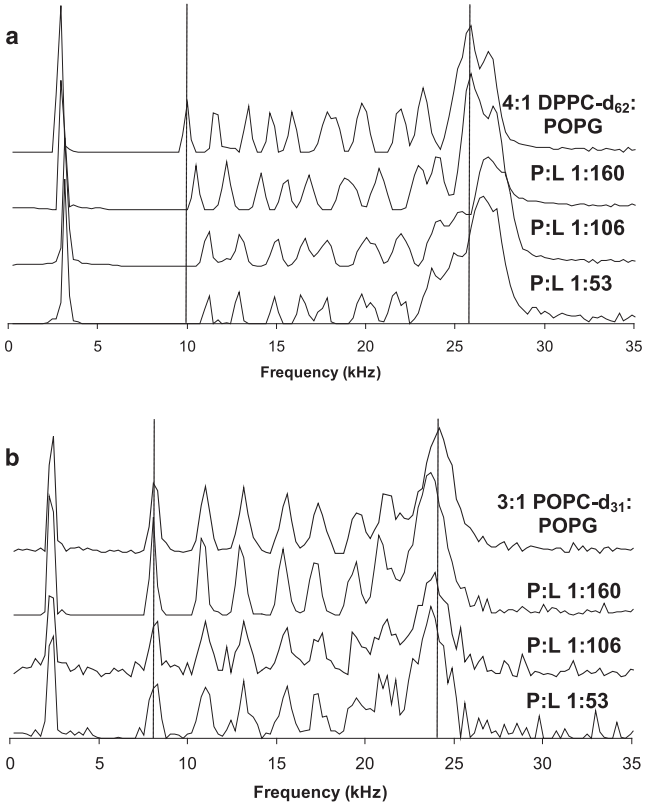

FIGURE 6 DePaked deuterium NMR spectra of (*top*) 4:1 DPPC-d_{62}/POPG and (*bottom*) 3:1 POPC-d_{31}/POPG MLVs with KL_4 at the indicated P/L ratios. Spectra were taken at 44°C.

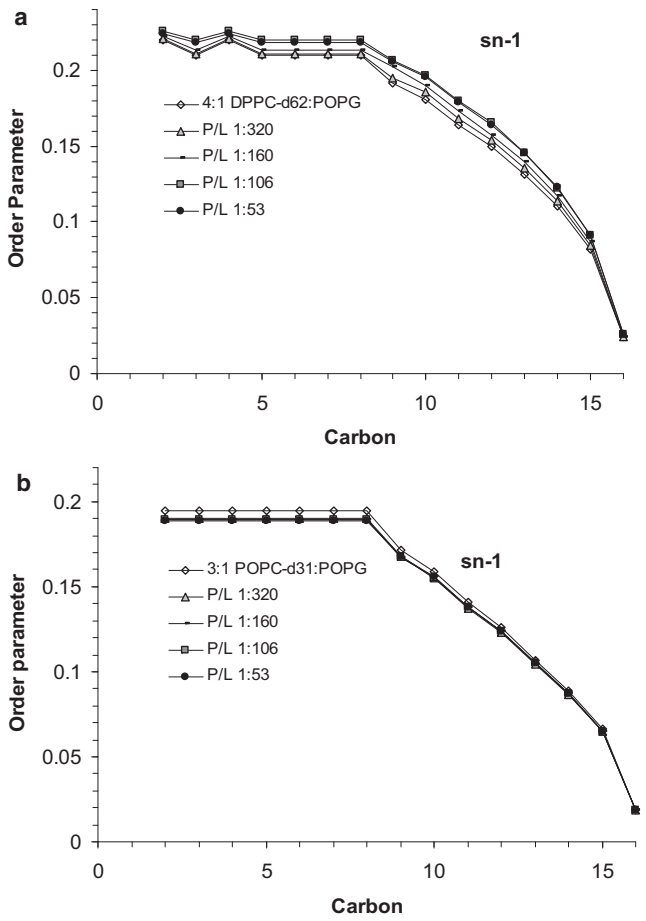

FIGURE 7 Order parameter profiles for the *sn*-1 chain of (*top*) DPPC-d_{62} in 4:1 DPPC-d_{62}/POPG and (*bottom*) POPC-d_{31} in 3:1 POPC-d_{31}/POPG MLVs with KL_4 at the indicated P/L ratios.

bilayer normal and the magnetic field. The overlaid powder patterns can be deconvoluted using a standard inversion (dePaking) procedure (60). For a sample in which the lipid bilayers show a tendency to align in the magnetic field, the probability distribution function must be adjusted. Assuming that the magnetic field leads to an ellipsoidal deformation of the MLVs, the probability distribution becomes (40):

$$p_{(E)}(\theta) \propto \sin(\theta)[1 - (1 - \kappa_E)\cos^2\theta]^{-2}. \quad (2)$$

Here κ_E refers to the square of the ratio of the long to short axes of the ellipsoids. Using an iterative procedure, which simultaneously determines κ_E and dePakes the spectrum, the order parameters, S_{CD}, can be determined with high accuracy in a partially aligned sample along with the degree of alignment. Order parameters calculated using deconvoluted spectra (Fig. 6) are tabulated in the Supporting Material; the resulting order parameter profiles are graphed in Fig. 7. The order parameter profiles clearly indicate that KL_4 has different effects on POPC versus DPPC lipids, with a small decrease in order for the POPC lipids and a larger increase in order for the DPPC lipids. The profiles also yield a more detailed picture of how KL_4 affects the lipid dynamics, with carbon positions 2–8 being the most affected in the POPC lipid acyl chains and positions 9–16 the most affected in the DPPC lipid acyl chains. The effects of KL_4 on the PG lipids were similarly monitored by collecting ^{2}H NMR spectra for 4:1 DPPC/POPG-d_{31} and 3:1 POPC/POPG-d_{31} MLVs and calculating the order parameter profiles for the *sn*-1 chain on POPG in these lipid mixtures (Supporting Material). In these experiments an overall decrease in ordering of the POPG acyl chains, particularly in the plateau region, is seen on addition of KL_4. Decreases in the order parameters are seen at all the acyl positions in POPG in 3:1 POPC/POPG MLVs and are greater than the changes for POPC in the plateau region. The POPG acyl chain order parameters in 4:1 DPPC/POPG MLVs do not appear to be as affected by KL_4; however, a comparison of the results further down the acyl chain for POPG-d_{31} when mixed with DPPC versus POPC again demonstrates that the peptide interacts with these lipid systems in a manner that depends on the degree of saturation of the fatty acid chains.

To clarify the effects of KL_4 on the individual lipids in the binary lipid mixtures, ^{2}H NMR spectra of neat lipids, DPPC-d_{62}, POPC-d_{31}, and POPG-d_{31}, with and without 1.5 mol % KL_4 were also collected, dePaked, and assigned (Supporting

Material). A comparison of these order parameter profiles with those for the lipids in binary mixtures shows that the DPPC order parameters for 4:1 DPPC/POPG MLVs with P/L ratios $>$ 1:200 are higher than would be expected for DPPC alone, and the POPG order parameters are also higher than expected for POPG alone. Within the resolution of the ^{2}H NMR experiment, no phase separation is seen. Thus, KL_4 is most likely interacting with both lipid populations in the fluid phase rather than segregating the lipids and interacting with a single phase above the L_β-to-L_α phase transition.

The observed changes in order parameters are seen more clearly when the data are viewed as the change in order parameter at each position along the acyl chain on addition of peptide relative to the order parameters of the lipids without the peptide. Shown in Fig. 8 are the changes in order parameters at particular methylene positions in the *sn*-1 palmitoyl acyl chains for the individual lipids in 3:1 POPC/POPG and 4:1 DPPC/POPG MLVs, respectively, on addition of peptide at a P/L molar ratio on the order of 1:100. From these graphs, the behavior of the PG lipids relative to the PC lipids is clearly offset, but the trends with respect to acyl chain position are similar. The offset of the profiles for the PG lipids is consistent with the ^{31}P NMR findings described above, showing that association of KL_4 with the lipids leads to a change in the orientation PG headgroups and an overall decrease in the ^{31}P CSAs for the POPG lipids. Thus, the offset in the PG profiles in Fig. 8 relative to the PC profiles does not reflect significantly less internal order in the PG lipid methylene chains per se, but instead reflects a change in the average orientation of the PG lipid director relative to the membrane normal.

The larger decrease in order parameters for POPG versus POPC in 3:1 POPC/POPG MLVs reflect the reorientation of the PG headgroup, and the lipid acyl chains are most likely equally affected in terms of the internal dynamics of the methylene chains. From their profiles, one can see that for this lipid system the methylenes in the plateau region are more affected than those further down the acyl chain. This behavior is somewhat in contrast to changes observed for antimicrobial peptides, which typically cause larger changes in order further down the methylene chain (37,61,62), and suggests that the interaction of KL_4 with monounsaturated lipids is unlike antimicrobial amphipathic helices, which have a much higher percentage of charged residues and are known to disrupt membrane bilayers. Changing the order of amino acids in the primary sequence of KL_4 to mimic a standard amphipathic α-helix abolishes its effectiveness as a surfactant (63). However, its behavior is similar to that of the C-terminus of SP-B, SP-B_{59-80} (64), and saposin C, a protein that is important for lipid enzymology and is closely related to SP-B (65,66).

Of particular interest regarding the role of KL_4 in lung surfactant formulations is its effects on 4:1 DPPC/POPG MLVs. From the order parameter profiles, one can see that KL_4 clearly increases in order along the DPPC acyl chains,

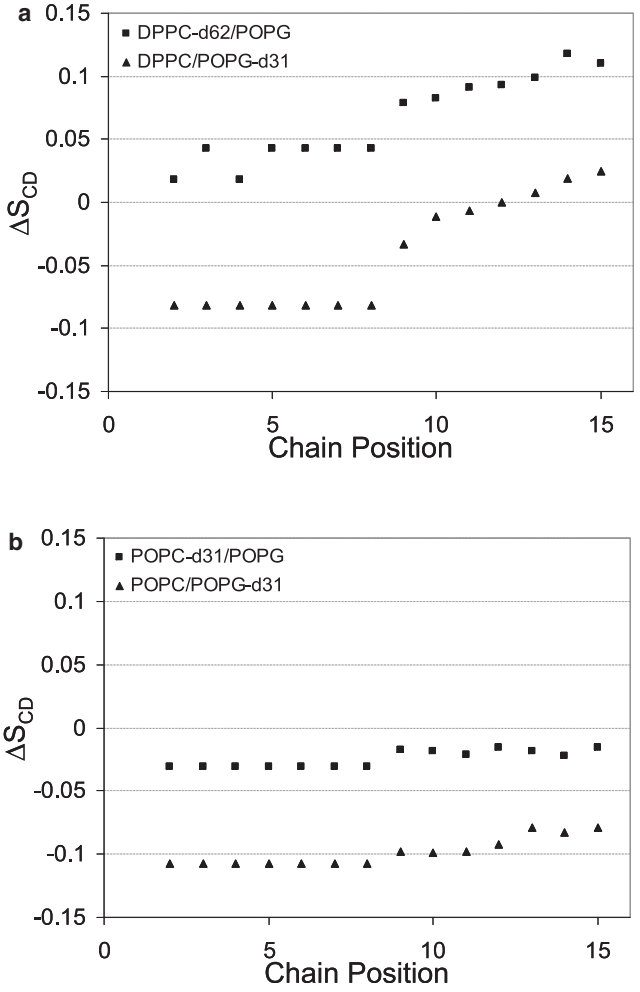

FIGURE 8 Changes in *sn-1* d_{31}-palmitoyl acid chain order parameters for PC lipids (*squares*), and POPG (*triangles*) in 4:1 DPPC/POPG MLVs (*top*) and 3:1 POPC/POPG (*bottom*).

with the greatest effect at the center of the bilayers. The profile for POPG also shows an increase toward the center of the bilayers but a decrease in the plateau region. However, as discussed above, the decrease reflects a change in the average orientation of the POPG headgroup, and if this change in orientation is taken into account, the internal order at individual methylene positions in the POPG acyl chain is increasing over the entire length of the acyl chain. We previously observed these same trends for SP-B_{59-80} (64). Similar behavior has also been observed on addition of the human antimicrobial peptide LL-37 to DMPC bilayers (61). Increases in lipid acyl chain ordering have been observed in response to polyelectrolyte binding to lipid headgroups (67,68), as well as in response to the addition of small molecules, such as cholesterol (69,70), or TM peptide helices that partition into the acyl chain region of the lipids (71,72). In the case of polyelectrolyte binding, larger changes are seen for the plateau region of the lipids, reflecting a change in overall orientation of the lipid packing and headgroups.

Smaller changes are also seen near the center of the bilayers and are interpreted as resulting from closer packing of the lipids on binding of the electrolyte. It is unlikely that KL_4 is affecting the lipid bilayers in this manner, since the ^{31}P results above show little change in the dynamics of the PC headgroups. For TM helices similar in length to KL_4, increases in order parameters that are similar in magnitude are seen for both the methylene positions in the plateau region and toward the center of the bilayers; these trends are observed in both POPC and DPPC bilayers. This is expected because insertion of a TM helical peptide primarily affects the thickness of the bilayer, and it would interact with both the lipid acyl chains and headgroups across the entire span of the bilayers. In contrast, for cholesterol, larger changes in order parameters are observed toward the center of the bilayer (69) because cholesterol partitions to the bilayer interior and does not strongly interact with the lipid head groups. The effects of KL_4 and SP-$B_{59–80}$ on the order parameters in DPPC/POPG bilayers are most similar to those of cholesterol. This suggests that the bulk of the peptides are partitioning deep within the lipid bilayers. The higher degree of ordering toward the center of the bilayer could be due to the leucines in KL_4 penetrating deeply into the bilayer and decreasing the mobility of the acyl chains. However, the smaller changes seen in the plateau region (carbons 3–8) suggest that the peptide does not adopt a TM orientation. These changes in order parameters indicate that KL_4 lodges into the hydrophobic region of the bilayer while maintaining its helix axis perpendicular to the bilayer normal. This type of interaction would lead to a negative curvature strain within the lipid bilayers, a phenomenon that has been hypothesized to be important for lung surfactant function (4). Of interest, ^2H spectra of 3:1 POPC/POPG lipid mixtures collected at 10°C (data not shown) show that KL_4 increases acyl chain order in a manner similar to that seen for 4:1 DPPC/POPG mixtures at 44°C. Thus, the contrast in the effects of KL_4 on lipid dynamics in the two lipid systems at physiologic temperatures is related to the difference between the temperature of observation and the phase transition temperatures of the individual lipid systems.

Another interesting outcome is seen when one compares the effect of KL_4 on DPPC and POPC acyl chains in mixed DPPC/POPG and POPC/POPG bilayers relative to the PC lipids alone (Fig. 9). Given the highly conserved lipid composition found in mammalian lung surfactants, POPG is most likely a critically important factor in the physical properties of surfactant. For both lipid systems, the incorporation of POPG leads to a greater change in the order parameter profiles of the PC lipids on addition of KL_4. Although the anionic POPG interacts with the peptide through electrostatic interactions with the lysine side chains, this interaction seems to increase the miscibility of the peptide with the PC lipids in the fluid phase rather than leading to phase separation, as evidenced by its increased effects on the PC lipid order parameters with addition of POPG.

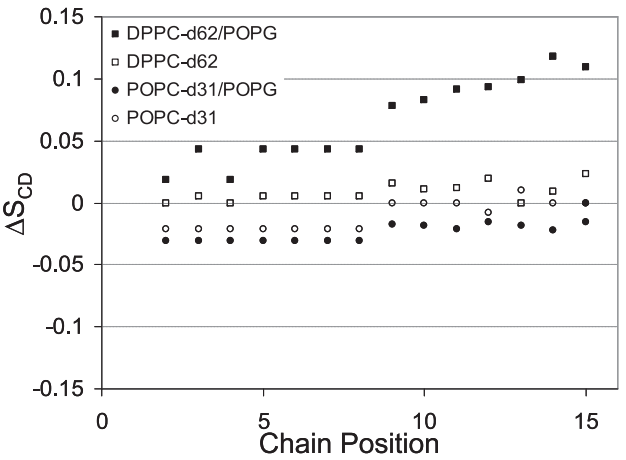

FIGURE 9 Changes in *sn*-1 d_{31}-palmitoyl acid chain order parameters for DPPC (*squares*) and POPC (*circles*) MLVs with (*closed symbols*) and without (*open symbols*) POPG on addition of KL_4 at P/L molar ratios of ~1:100.

Binding and insertion depth of KL_4 into lipid bilayers

To more directly gauge the insertion depth of KL_4 into the DPPC/POPG and POPC/POPG bilayers, samples were prepared for ^1H spin diffusion experiments. For these experiments, the peptide was $^{13}C'$ enriched at positions L9 and L10, and initial CPMAS spectra were collected to assess the dynamics and cross-polarization efficiency of the peptide (Fig. 10 *a*). The sample containing DPPC affords high-quality CPMAS spectra with an easily discernible $^{13}C'$ resonance at 172 ppm. However, ^{13}C' resonances are not as clearly seen in the CPMAS spectra for the sample containing POPC at 25°C and 40°C, and cross polarization is less efficient. Cooling the samples down to nearer the phase transition temperature of the lipids leads to the appearance of peptide $^{13}C'$ signal at 174 ppm. Thus the peptide is clearly bound and immobilized in the fluid-phase DPPC/POPG bilayers on the NMR timescale, but when interacting with the POPC/POPG bilayers at physiologic temperatures it is only transiently bound or highly mobile. This contrasts with previous observations of the binding of KL_4 to POPC/POPG LUVs in 5 mM HEPES buffer alone (73). Similar variations in peptide dynamics for a peptide ion channel mixed with lipids in organic solvents or bound to lipid LUVs from buffer have been observed (74). Of interest, these differences in dynamics do not necessarily correlate to global changes in secondary structure, as the isotropic chemical shifts for enriched $^{13}C'$ positions in KL_4 in the two POPC/POPG sample preparations are indistinguishable when the samples are flash-frozen (at ~172 ppm) and the two preparations yield similar CD spectra. However, we do see a slight change in the isotropic chemical shifts between the two POPC/POPG preparations when the lipids are in the fluid phase: the more dynamic preparation, resulting

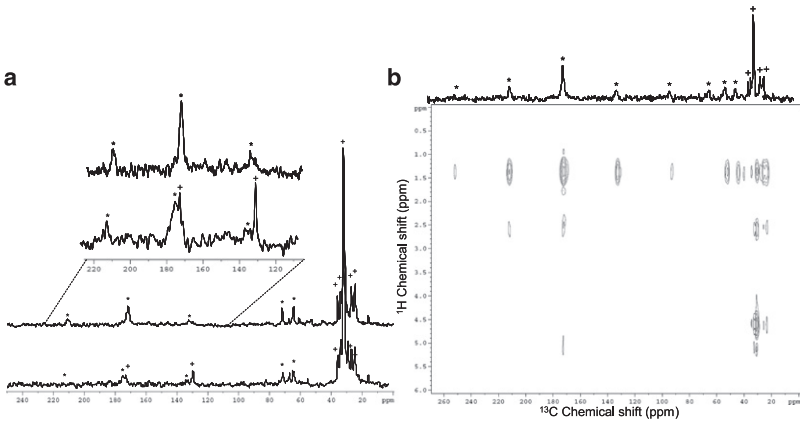

FIGURE 10 (*Left*) CPMAS spectra of KL_4 in 4:1 DPPC: POPG vesicles (*top*), collected at 40°C, and 3:1 POPC: POPG vesicles (*bottom*), collected near 0°C, at a P/L molar ratio of 1:33. The peptide is $^{13}C'$-enriched at positions L9 and L10. Peptide resonances (*) and lipid resonances (+) are indicated. In the expansion of the region for the $^{13}C'$ isotropic and first spinning sideband resonances, the attenuation of peptide signal in 3:1 POPC/POPG vesicles can be seen and the lipid signals are more prevalent. (*Right*) 2D ^{13}C-detected ^{1}H spin-diffusion spectrum for 1:33 KL_4 in 4:1 DPPC/POPG with the peptide (*) and lipid (+) ^{13}C resonances indicated in the $t_1 = 0$ experiment (*top*).

from mixing KL_4 with lipids in an organic phase, has an isotropic chemical shift near 174 ppm (Fig. 10 *a*), whereas the less dynamic preparation has an isotropic chemical shift of 172 ppm (73). Carbonyl $^{13}C'$ signals are particularly susceptible to slight variations in hydration and/or hydrogen bonding (75), which would explain these observations. The transient nature of the KL_4 interactions with the POPC/POPG bilayers would also explain why its effects on acyl chain order are attenuated relative to its effects on order in DPPC/POPG bilayers.

The interaction of KL_4 with the DPPC/POPG bilayers in the fluid phase was characterized by means of ^{1}H spin diffusion experiments. Fig. 10 *b* shows a representative ^{13}C-detected ^{1}H spin diffusion spectrum at a mixing time of 100 ms, in which an interaction of the peptide $^{13}C'$ resonances at ~172 ppm with the lipid acyl chains at a ^{1}H chemical shift of 1.3 ppm is clearly seen. Although the lipids are also exchanging polarization with water, as evidenced by a cross-peak at a ^{1}H chemical shift of 4.7 ppm and a ^{13}C chemical shift of 30 ppm, no appreciable signal corresponding to spin diffusion between the peptide and water is seen. This observation is consistent with the peptide penetrating deeply into the lipid bilayers (43).

DISCUSSION

The dynamic air-fluid interface in the lung requires lung surfactant to possess specific attributes to lower surface tension and allow rapid respreading of lipids. Lung surfactant relies on relatively low levels of lung surfactant proteins B and C (<0.2 mol %) to alter the structure, dynamics, and phase properties of the lipids. The peptide KL_4 similarly affects the macroscopic properties of the lipids and has been pursued as a clinical replacement for SP-B in therapeutic formulations (30,33). However, the molecular mechanisms behind its properties have not been fully elucidated. FTIR measurements of SP-B interacting with lipid bilayers indicate that it is a helical protein with the helices oriented perpendicular to the membrane normal (19,20). FTIR studies of KL_4 in which the amide I′ band was monitored led to conflicting models of the structure and orientation of the peptide. In early work using oriented bilayers at limited hydration, investigators concluded that KL_4 was helical in 7:3 DPPC/DPPG but spanned the bilayers (76). Later work with DPPC and DPPG mixed monolayers at an air-water interface indicated that KL_4 lies along the surface of the lipids as a mixture of helix and sheet (77). However, in both of these studies it was assumed that KL_4 forms either a classic α-helical or β-sheet secondary structure with standard backbone conformations and hydrogen-bonding distances. Additionally, the amide I′ band is sensitive to the solvation environment of the peptide being monitored, and thus variable partitioning into the lipid environments could explain the observed changes in stretching frequencies. More recently, an in vitro transcription-translation system, which utilizes the *Escherichia coli* inner membrane protein leader peptidase (Lep) to report on the integration of TM helices into ER membranes, was used to assay whether KL_4 or SP-$B_{59–80}$ would partition as TM helices in the context of a Lep model protein (78). In that study, KL_4 was found to incorporate into the protein as a TM helix whereas SP-$B_{59–80}$ did not. However, the accuracy of this host-guest system for predicting the partitioning of positively charged amphipathic sequences has been called into question given the complexity of the translocon protein assembly and mechanisms of glycosylation (79–81). The possible secondary structures of KL_4, as well as its interactions with specific lipids found in lung surfactant, need more thorough examination. In an attempt to gain a molecular-level understanding of how KL_4 alters lipid properties, we undertook an ssNMR examination of how KL_4 interacts with two lipid formulations: 4:1 DPPC/POPG and 3:1 POPC/POPG.

Our CD measurements, as well as previously published work (46), show KL_4 to be helical in both POPC/POPG and DPPC/POPG lipid mixtures. However, in all probability, KL_4 does not form a classic α-helix if the helix axis is perpendicular to the membrane normal, since this would place the lysines evenly around the helix (Fig. 2 *A*). Lysine- and leucine-rich peptides have been shown to adopt different amphipathic secondary structures at the air-water interface

and on polymer surfaces based on the amino acid pattern of the residues (82,83). Similar driving forces would exist at the lipid bilayer surface. A possible explanation for how KL_4 partitions as a helix into the bilayers is that it may form a structure in which the lysines lie on one side of a helix. The length and flexibility of the lysine side chains would allow either an amphipathic helical conformation of KL_4, which preferentially binds at the lipid interface (Fig. 2 *B*), or a π-helix conformation in which the peptide deeply penetrates into the bilayer while retaining electrostatic interactions between the lysine side chains and the lipid phosphate groups by ''snorkeling'' (Fig. 2 *C*). We recently determined the structure of KL_4 in 3:1 POPC/POPG MLVs via ssNMR dipolar recoupling experiments (73). The average backbone torsion angles found were $(-105, -30)$, which allow KL_4 to form an amphipathic helix in which the lysines lie on one half of the peptide helix as in Fig. 2 *B*. This would allow the peptide to preferentially interact with the lipids at the bilayer interface, but would make deeper penetration into the hydrophobic region of the lipids unfavorable. Measurements of the structure of KL_4 in DPPC/POPG MLVs suggest i to $i + 5$ hydrogen bonding (A. K. Mehta and J. R. Long, unpublished data). Of interest, the CD spectrum for KL_4 interacting with DPPC/POPG LUVs is very similar to that observed for recently published peptides that are constrained by covalent bonds to form π-helices (44).

Another consideration is whether the helical form of KL_4 might span the bilayers in a TM conformation. The snorkeling of lysine residues was previously postulated to stabilize the TM WALP and KALP peptides (84). However, the length of the lysine side chain limits its placement relative to the peptide termini for a TM orientation to be observed. Of specific interest regarding the orientation of KL_4 are the 22 amino acid peptides KKLLKLLLLLLLLLKLLLLKK and KKLLLLLKLLLLLLLKLLLLKK, which have been characterized in POPC membranes. The former peptide adopts a TM orientation, whereas the latter peptide exchanges slowly between different orientations in the bilayers (85). These peptides bear a striking homology to KL_4 in both amino acid content and hydrophobic to hydrophilic ratio, but only the sequence in which the lysines are distributed more toward the termini is able to achieve a stable TM configuration. The thermodynamic penalty imposed by placing KL_4 in a TM orientation would be prohibitive since it would result in charged amino acids partitioned into the hydrophobic core. Thus KL_4 most likely binds lipid membranes in an amphipathic helical conformation with the helix axis parallel to the plane of the bilayers. This orientation is supported by comparison of the effects of KL_4 and SP-B_{59-80} on lipid dynamics (86). Both peptides yield strikingly similar results when the changes in the dynamics of fully hydrated POPC/POPG and DPPC/POPG mixtures are examined, and their effects are somewhat similar to those of the antimicrobial peptide LL-37 at low peptide/lipid ratios (61). It has been established that both LL-37 and SP-B_{59-80} form helical structures at lipid interfaces rather than spanning lipid bilayers. In all likelihood, the studies that found KL_4 to adopt a TM orientation suffered from the conditions of the experiments; however, it is likely that deep partitioning of the peptide into the membrane is energetically more favorable, and this may be a key feature in its function within lung surfactant.

The variation in the amphipathic helical structure of KL_4 sets it apart from classic amphipathic α-helices. Cationic, leucine-rich amphipathic helical peptides have been pursued as antimicrobial agents because their positive charge leads to preferential targeting of the anionic-rich membranes typical of prokaryotes (87). These peptides are specifically intended to form amphipathic α-helices based on naturally occurring antimicrobial peptides, and disrupt membranes on binding through the carpet mechanism or the formation of toroidal or barrel stave pores (87–89). However, these peptides have a significantly higher percentage of charged residues (>50% vs. <25% for KL_4), and the periodicity of the hydrophobic and hydrophilic residues is designed to favor classic amphipathic α-helices. We find no indication of membrane disruption by KL_4, consistent with the notion that its mechanism of interaction with lipids differs from that of antimicrobial peptides. The higher hydrophobicity of the amphipathic KL_4 helices modeled in Fig. 2 would favor more interaction with the lipid acyl chains relative to the lipid headgroups and thus would exert less positive curvature strain on the lipid bilayers.

Our data on lipid dynamics support our conclusions regarding the helical structure and orientation of KL_4. In POPC/POPG bilayers, a decrease in acyl chain order on addition of peptide suggests partitioning of the peptide into the lipid headgroup region. The acyl chain ordering in the DPPC/POPG lipids is more marked at positions 9–15 than in the plateau region, suggesting deep penetration of the peptide into the lipid bilayer with less perturbation of the headgroup region than is seen for leucine-rich TM helices. A π-helical conformation with snorkeling of the lysines would allow KL_4 to penetrate more deeply into saturated lipid bilayers while remaining perpendicular to the bilayer normal.

The proposed snorkeling of KL_4 within DPPC/POPG lipid multilamellar vesicles would have important consequences for membrane structure and function. This represents a novel peptide-lipid interaction that is unusual in comparison to what has been seen for membrane active amphipathic α-helices. Although the binding of KL_4 to POPC/POPG vesicles suggests that it could bind to these lipids in a manner similar to amphipathic α-helices, its ability to snorkel in DPPC/POPG lipids would have a different effect on lipid biophysics, particularly in the alveoli. Some of the thermodynamic costs of peptide penetration can be relieved by the formation of alternative nonlamellar structures, such as hexagonal phases (90,91). The formation of alternative lipid geometries, specifically the inverted H_{II} phase, has been found to be important for lung surfactant function (4). It has also been hypothesized that SP-B causes negative curvature strain in lung surfactant

and may even favor the formation of a hexagonal phase. Although we did not observe a hexagonal phase in this study, the partitioning of KL_4 deep into the DPPC/POPG bilayers would significantly increase negative curvature strain. The addition of small levels of cholesterol or POPE could further affect the curvature strain in the lipid bilayers and cause the formation of a hexagonal phase. Studies of the effect of KL_4 on other model lung surfactant compositions are ongoing. Preliminary work with DPPE/POPG lipids indicates that KL_4 promotes the formation of the H_{II} phase at lower temperatures. Alternatively, lipid geometry could be critical during fusion of lipids to the air-surfactant interface, and KL_4 snorkeling could be an essential feature for the proper shuttling of lipids. Our studies also highlight that the properties of KL_4 are lipid-dependent, and thus KL_4 could play a role in differential lipid partitioning to the air-water interface.

CONCLUSIONS

The unique interplay among lipid saturation, peptide penetration, and peptide structure we observed could explain the unique properties of KL_4 in the dynamic lung environment. DSC, ^{31}P, ^{2}H, ^{13}C CPMAS, and ^{1}H spin diffusion data all indicate that KL_4 binds peripherally to 3:1 POPC/POPG lipids through electrostatic interaction of the lipid phosphates with the positively charged lysines. A different interaction is seen with 4:1 DPPC/POPG lipids, suggesting that the peptide penetrates to a far greater depth in the bilayer. CD measurements indicate that the peptide is helical in both lipid environments, although the amount and character of the helix are lipid-dependent; alterations in helix pitch would allow KL_4 to adapt its structure to match the environment for different insertion depths. Thus, both peptide structural plasticity and acyl chain saturation play an important role in determining the insertion level of KL_4. The variations in peptide penetration would directly affect the stability and composition of lipid structures in lung surfactant by increasing positive curvature strain in POPC-enriched domains and increasing negative curvature strain in DPPC-enriched domains. These changes in curvature strain would provide a mechanism for lipid trafficking from lamellar bodies and tubular myelin to the air-water interface in a manner selective for DPPC. The enrichment of DPPC at the air-water interface has been postulated to be one of the major roles of SP-B. The plasticity of KL_4 in its structure and insertion depth could be a consequence of the spacing of hydrophilic amino acids every five residues; the paucity of aromatic residues, which favor partitioning to the lipid interface; the high percentage of leucine residues, which favors interactions with lipid acyl chains; the choice of lysines for the charged amino acids, which allows for side-chain snorkeling; or a combination of these factors. The importance of each of these characteristics to the partitioning, insertion, and structure of amphipathic helices relevant to lung surfactant is the subject of ongoing studies. With the findings presented here, a more thorough molecular model can be established to explain how this small peptide modulates lipid properties and drive the development of future SP-B mimetics.

SUPPORTING MATERIAL

Eight figures and five tables are available at http://www.biophysj.org/biophysj/supplemental/S0006-3495(09)00667-5.

We thank Profs. Art Edison, Gail Fanucci, and Manish Mehta for helpful discussions, and Dr. Omjoy Ganesh for editing assistance. The assistance of Dr. Alfred Chung in peptide synthesis and the Molecular Structure Facility at University of California, Davis, in AAA analysis is gratefully acknowledged.

This research was funded by the National Institutes of Health (1R01HL076586 to J.R.L.). Support from the National Science Foundation's National High Magnetic Field Laboratory and the University of Florida is also gratefully acknowledged. E.S. received financial support from the Natural Sciences and Engineering Research Council of Canada.

REFERENCES

1. Goerke, J. 1998. Pulmonary surfactant: functions and molecular composition. *Biochim. Biophys. Acta.* 1408:79–89.
2. Whitsett, J. A., and T. E. Weaver. 2002. Hydrophobic surfactant proteins in lung function and disease. *N. Engl. J. Med.* 347:2141–2148.
3. Cullis, P. R., and B. de Kruijff. 1979. Lipid polymorphism and the functional roles of lipids in biological membranes. *Biochim. Biophys. Acta.* 559:399–420.
4. Perkins, W. R., R. B. Dause, R. A. Parente, S. R. Minchey, K. C. Neuman, et al. 1996. Role of lipid polymorphism in pulmonary surfactant. *Science.* 273:330–332.
5. Veldhuizen, R., K. Nag, S. Orgeig, and F. Possmayer. 1998. The role of lipids in pulmonary surfactant. *Biochim. Biophys. Acta.* 1408:90–108.
6. Postle, A. D., E. L. Heeley, and D. C. Wilton. 2001. A comparison of the molecular species compositions of mammalian lung surfactant phospholipids. *Comp. Biochem. Physiol. A Mol. Integr. Physiol.* 129:65–73.
7. Weaver, T. E., and J. A. Whitsett. 1991. Function and regulation of expression of pulmonary surfactant-associated proteins. *Biochem. J.* 273:249–264.
8. Whitsett, J. A., L. M. Nogee, T. E. Weaver, and A. D. Horowitz. 1995. Human surfactant protein-B—structure, function, regulation, and genetic-disease. *Physiol. Rev.* 75:749–757.
9. Clark, J. C., S. E. Wert, C. J. Bachurski, M. T. Stahlman, B. R. Stripp, et al. 1995. Targeted disruption of the surfactant protein B gene disrupts surfactant homeostasis, causing respiratory failure in newborn mice. *Proc. Natl. Acad. Sci. USA.* 92:7794–7798.
10. Nogee, L. M., D. E. Demello, L. P. Dehner, and H. R. Colten. 1993. Brief report—deficiency of pulmonary surfactant protein-B in congenital alveolar proteinosis. *N. Engl. J. Med.* 328:406–410.
11. Hamvas, A. 2006. Inherited surfactant protein-B deficiency and surfactant protein-C associated disease: clinical features and evaluation. *Semin. Perinatol.* 30:316–326.
12. Ballard, P. L., J. D. Merrill, R. I. Godinez, M. H. Godinez, W. E. Truog, et al. 2003. Surfactant protein profile of pulmonary surfactant in premature infants. *Am. J. Respir. Crit. Care Med.* 168:1123–1128.
13. Weaver, T. E., and J. J. Conkright. 2001. Function of surfactant proteins B and C. *Annu. Rev. Physiol.* 63:555–578.
14. Robertson, B., and H. L. Halliday. 1998. Principles of surfactant replacement. *Biochim. Biophys. Acta.* 1408:346–361.
15. Jobe, A. H. 1993. Drug-therapy—pulmonary surfactant therapy. *N. Engl. J. Med.* 328:861–868.

16. Sarin, V. K., S. Gupta, T. K. Leung, V. E. Taylor, B. L. Ohning, et al. 1990. Biophysical and biological-activity of a synthetic 8.7-kda hydrophobic pulmonary surfactant protein SP-B. *Proc. Natl. Acad. Sci. USA.* 87:2633–2637.

17. Revak, S. D., T. A. Merritt, M. Hallman, G. Heldt, R. J. Lapolla, et al. 1991. The use of synthetic peptides in the formation of biophysically and biologically-active pulmonary surfactants. *Pediatr. Res.* 29:460–465.

18. Johansson, J., and T. Curstedt. 1997. Molecular structures and interactions of pulmonary surfactant components. *Eur. J. Biochem.* 244:675–693.

19. Vandenbussche, G., A. Clercx, M. Clercx, T. Curstedt, J. Johansson, et al. 1992. Secondary structure and orientation of the surfactant protein SP-B in a lipid environment—a Fourier-transform infrared-spectroscopy study. *Biochemistry.* 31:9169–9176.

20. Wustneck, N., R. Wustneck, J. Perez-Gil, and U. Pison. 2003. Effects of oligomerization and secondary structure on the surface behavior of pulmonary surfactant proteins SP-B and SP-C. *Biophys. J.* 84:1940–1949.

21. Hall, S. B., Z. Wang, and R. H. Notter. 1994. Separation of subfractions of the hydrophobic components of calf lung surfactant. *J. Lipid Res.* 35:1386–1394.

22. Gustafsson, M., T. Curstedt, H. Jornvall, and J. Johansson. 1997. Reverse-phase HPLC of the hydrophobic pulmonary surfactant proteins: detection of a surfactant protein C isoform containing *n*-epsilon-palmitoyl-lysine. *Biochem. J.* 326:799–806.

23. Baatz, J. E., Y. Zou, J. T. Cox, Z. Wang, and R. H. Notter. 2001. High-yield purification of lung surfactant proteins SP-B and SP-C and the effects on surface activity. *Protein Expr. Purif.* 23:180–190.

24. Mingarro, I., D. Lukovic, M. Vilar, and J. Perez-Gil. 2008. Synthetic pulmonary surfactant preparations: new developments and future trends. *Curr. Med. Chem.* 15:393–403.

25. Seurynck, S. L., J. A. Patch, and A. E. Barron. 2005. Simple, helical peptoid analogs of lung surfactant protein B. *Chem. Biol.* 12:77–88.

26. Cochrane, C. G., and S. D. Revak. 1991. Pulmonary surfactant protein B (SP-B): structure-function relationships. *Science.* 254:566–568.

27. Cochrane, C. G., S. D. Revak, A. Merritt, G. P. Heldt, M. Hallman, et al. 1996. The efficacy and safety of kl(4)-surfactant in infants with respiratory distress syndrome. *Am. J. Respir. Crit. Care Med.* 153:404–410.

28. Cochrane, C. G., S. D. Revak, T. A. Merritt, I. U. Schraufstatter, R. C. Hoch, et al. 1998. Bronchoalveolar lavage with kl4-surfactant in models of meconium aspiration syndrome. *Pediatr. Res.* 44:705–715.

29. Wiswell, T. E., R. M. Smith, L. B. Katz, L. Mastroianni, D. Y. Wong, et al. 1999. Bronchopulmonary segmental lavage with surfaxin (kl4-surfactant) for acute respiratory distress syndrome. *Am. J. Respir. Crit. Care Med.* 160:1188–1195.

30. Sinha, S. K., T. Lacaze-Masmonteil, A. V. I. Soler, T. E. Wiswell, J. Gadzinowski, et al. 2005. A multicenter, randomized, controlled trial of lucinactant versus poractant alfa among very premature infants at high risk for respiratory distress syndrome. *Pediatrics.* 115:1030–1038.

31. Ghodrat, M. 2006. Lung surfactants. *Am. J. Health Syst. Pharm.* 63:1504–1521.

32. Cochrane, C. G., and S. D. Revak. 1994. Protein-phospholipid interactions in pulmonary surfactant. The Parker B. Francis Lectureship. *Chest.* 105:57S–62S.

33. Moya, F. R., J. Gadzinowski, E. Bancalari, V. Salinas, B. Kopelman, et al. 2005. A multicenter, randomized, masked, comparison trial of lucinactant, colfosceril palmitate, and beractant for the prevention of respiratory distress syndrome among very preterm infants. *Pediatrics.* 115:1018–1029.

34. Kinniry, P., J. Pick, S. Stephens, D. Jain, C. C. Solomides, et al. 2006. Kl4-surfactant prevents hyperoxic and LPS-induced lung injury in mice. *Pediatr. Pulmonol.* 41:916–928.

35. Ryan, M. A., H. T. Akinbi, A. G. Serrano, J. Perez-Gil, H. X. Wu, et al. 2006. Antimicrobial activity of native and synthetic surfactant protein B peptides. *J. Immunol.* 176:416–425.

36. Terzi, E., G. Holzemann, and J. Seelig. 1997. Interaction of Alzheimer β-amyloid peptide(1–40) with lipid membranes. *Biochemistry.* 36:14845–14852.

37. Ramamoorthy, A., S. Thennarasu, D. K. Lee, A. Tan, and L. Maloy. 2006. Solid-state NMR investigation of the membrane-disrupting mechanism of antimicrobial peptides msi-78 and msi-594 derived from magainin 2 and melittin. *Biophys. J.* 91:206–216.

38. Wieprecht, T., O. Apostolov, M. Beyermann, and J. Seelig. 1999. Thermodynamics of the α-helix-coil transition of amphipathic peptides in a membrane environment: implications for the peptide-membrane binding equilibrium. *J. Mol. Biol.* 294:785–794.

39. Chen, P. S., T. Y. Toribara, and H. Warner. 1956. Microdetermination of phosphorus. *Anal. Chem.* 28:1756–1758.

40. Sternin, E., H. Schafer, I. V. Polozov, and K. Gawrisch. 2001. Simultaneous determination of orientational and order parameter distributions from NMR spectra of partially oriented model membranes. *J. Magn. Reson.* 149:110–113.

41. Petrache, H. I., S. W. Dodd, and M. F. Brown. 2000. Area per lipid and acyl length distributions in fluid phosphatidylcholines determined by (2)h NMR spectroscopy. *Biophys. J.* 79:3172–3192.

42. Seelig, A., and J. Seelig. 1974. The dynamic structure of fatty acyl chains in a phospholipid bilayer measured by deuterium magnetic resonance. *Biochemistry.* 13:4839–4845.

43. Huster, D., X. L. Yao, and M. Hong. 2002. Membrane protein topology probed by H-1 spin diffusion from lipids using solid-state NMR spectroscopy. *J. Am. Chem. Soc.* 124:874–883.

44. Chapman, R., J. L. Kulp, A. Patgiri, N. R. Kallenbach, C. Bracken, et al. 2008. Trapping a folding intermediate of the α-helix: stabilization of the pi-helix. *Biochemistry.* 47:4189–4195.

45. Andrade, M. A., P. Chacon, J. J. Merelo, and F. Moran. 1993. Evaluation of secondary structure of proteins from UV circular-dichroism spectra using an unsupervised learning neural-network. *Protein Eng.* 6:383–390.

46. Saenz, A., O. Canadas, L. A. Bagatolli, M. E. Johnson, and C. Casals. 2006. Physical properties and surface activity of surfactant-like membranes containing the cationic and hydrophobic peptide kl4. *FEBS J.* 273:2515–2527.

47. Ma, J. W., S. Koppenol, H. U. Yu, and G. Zografi. 1998. Effects of a cationic and hydrophobic peptide, kl4, on model lung surfactant lipid monolayers. *Biophys. J.* 74:1899–1907.

48. Liu, F., R. N. A. H. Lewis, R. S. Hodges, and R. N. McElhaney. 2002. Effect of variations in the structure of a polyleucine-based α-helical transmembrane peptide on its interaction with phosphatidylcholine bilayers. *Biochemistry.* 41:9197–9207.

49. Seelig, J. 1978. ^{31}P nuclear magnetic resonance and the head group structure of phospholipids in membranes. *Biochim. Biophys. Acta.* 515:105–140.

50. Qiu, X., P. A. Mirau, and C. Pidgeon. 1993. Magnetically induced orientation of phosphatidylcholine membranes. *Biochim. Biophys. Acta.* 1147:59–72.

51. Reinl, H., T. Brumm, and T. M. Bayerl. 1992. Changes of the physical-properties of the liquid-ordered phase with temperature in binary-mixtures of DPPC with cholesterol—a H-2-NMR, FT-IR, DSC, and neutron-scattering study. *Biophys. J.* 61:1025–1035.

52. Ouellet, M., G. Bernard, N. Voyer, and M. Auger. 2006. Insights on the interactions of synthetic amphipathic peptides with model membranes as revealed by ^{31}P and ^{2}H solid-state NMR and infrared spectroscopies. *Biophys. J.* 90:4071–4084.

53. Lu, J. X., J. Blazyk, and G. A. Lorigan. 2006. Exploring membrane selectivity of the antimicrobial peptide kigaki using solid-state NMR spectroscopy. *Biochim. Biophys. Acta.* 1758:1303–1313.

54. Pott, T., and E. J. Dufourc. 1995. Action of melittin on the DPPC-cholesterol liquid-ordered phase: a solid state ^{2}H-and ^{31}P-NMR study. *Biophys. J.* 68:965–977.

55. Bechinger, B. 2005. Detergent-like properties of magainin antibiotic peptides: a ^{31}P solid-state NMR spectroscopy study. *Biochim. Biophys. Acta.* 1712:101–108.

56. Naito, A., T. Nagao, M. Obata, Y. Shindo, M. Okamoto, et al. 2002. Dynorphin induced magnetic ordering in lipid bilayers as studied by P-31 NMR spectroscopy. *Biochim. Biophys. Acta.* 1558:34–44.

57. Bunow, M. R., and I. W. Levin. 1977. Raman-spectra and vibrational assignments for deuterated membrane lipids—1,2-dipalmitoyl phosphatidylcholine-d9 and 1,2-dipalmitoyl phosphatidylcholine-d62. *Biochim. Biophys. Acta.* 489:191–206.

58. Seelig, J., and A. Seelig. 1980. Lipid conformation in model membranes and biological membranes. *Q. Rev. Biophys.* 13:19–61.

59. Burnett, L. J., and B. H. Muller. 1971. Deuteron quadrupole coupling constants in 3 solid deuterated paraffin hydrocarbons—c2d6, c4d10, c6d14. *J. Chem. Phys.* 55:5829–5831.

60. Sternin, E., M. Bloom, and A. L. Mackay. 1983. De-pake-ing of NMR-spectra. *J. Magn. Reson.* 55:274–282.

61. Henzler-Wildman, K. A., G. V. Martinez, M. F. Brown, and A. Ramamoorthy. 2004. Perturbation of the hydrophobic core of lipid bilayers by the human antimicrobial peptide ll-37. *Biochemistry.* 43:8459–8469.

62. Porcelli, F., B. Buck, D. K. Lee, K. J. Hallock, A. Ramamoorthy, et al. 2004. Structure and orientation of pardaxin determined by NMR experiments in model membranes. *J. Biol. Chem.* 279:45815–45823.

63. Nilsson, G., M. Gustafsson, G. Vandenbussche, E. Veldhuizen, W. J. Griffiths, et al. 1998. Synthetic peptide-containing surfactants—evaluation of transmembrane versus amphipathic helices and surfactant protein C poly-valyl to poly-leucyl substitution. *Eur. J. Biochem.* 255:116–124.

64. Antharam, V. C., R. S. Farver, A. Kuznetsova, K. H. Sippel, F. D. Mills, et al. 2008. Interactions of the C-terminus of lung surfactant protein B with lipid bilayers are modulated by acyl chain saturation. *Biochim. Biophys. Acta.* 1778:2544–2554.

65. Abu-Baker, S., X. Y. Qi, and G. A. Lorigan. 2007. Investigating the interaction of saposin C with POPS and POPC phospholipids: a solid-state NMR spectroscopic study. *Biophys. J.* 93:3480–3490.

66. Abu-Baker, S., X. Y. Qi, J. Newstadt, and G. A. Lorigan. 2005. Structural changes in a binary mixed phospholipid bilayer of DOPG and DOPS upon saposin C interaction at acidic pH utilizing P-31 and H-2 solid-state NMR spectroscopy. *Biochim. Biophys. Acta.* 1717:58–66.

67. Huster, D., U. Dietrich, T. Gutberlet, K. Gawrisch, and K. Arnold. 2000. Lipid matrix properties in cationic membranes interacting with anionic polyelectrolytes: a solid-state NMR approach. *Langmuir.* 16:9225–9232.

68. Laroche, G., E. J. Dufourc, M. Pezolet, and J. Dufourcq. 1990. Coupled changes between lipid order and polypeptide conformation at the membrane-surface—a H-2 NMR and Raman study of polylysine phosphatidic-acid systems. *Biochemistry.* 29:6460–6465.

69. Stockton, G. W., and I. C. P. Smith. 1976. Deuterium nuclear magnetic-resonance study of condensing effect of cholesterol on egg phosphatidylcholine bilayer membranes. 1. Perdeuterated fatty-acid probes. *Chem. Phys. Lipids.* 17:251–263.

70. Oldfield, E., M. Meadows, D. Rice, and R. Jacobs. 1978. Spectroscopic studies of specifically deuterium labeled membrane systems—nuclear magnetic-resonance investigation of effects of cholesterol in model systems. *Biochemistry.* 17:2727–2740.

71. Nezil, F. A., and M. Bloom. 1992. Combined influence of cholesterol and synthetic amphiphillic peptides upon bilayer thickness in model membranes. *Biophys. J.* 61:1176–1183.

72. de Planque, M. R., D. V. Greathouse, R. E. Koeppe, 2nd, H. Schafer, D. Marsh, et al. 1998. Influence of lipid/peptide hydrophobic mismatch on the thickness of diacylphosphatidylcholine bilayers. A ^{2}H NMR and ESR study using designed transmembrane α-helical peptides and gramicidin a. *Biochemistry.* 37:9333–9345.

73. Mills, F. D., V. C. Antharam, D. W. Elliott, S. A. McNeill, and J. R. Long. 2008. The helical structure of surfactant peptide kl4 when bound to POPC:POPG lipid vesicles. *Biochemistry.* 47:8292–8300.

74. Cady, S. D., and M. Hong. 2008. Amantadine-induced conformational and dynamical changes of the influenza m2 transmembrane proton channel. *Proc. Natl. Acad. Sci. USA.* 105:1483–1488.

75. Kameda, T., and I. Ando. 1997. The relationship between the helical conformation and C-13 NMR chemical shift of amino acid residue carbonyl carbons of polypeptides in the solid state. *J. Mol. Struct.* 412:197–203.

76. Gustafsson, M., G. Vandenbussche, T. Curstedt, J. M. Ruysschaert, and J. Johansson. 1996. The 21-residue surfactant peptide (lysleu4)4lys(kl4) is a transmembrane α-helix with a mixed nonpolar/polar surface. *FEBS Lett.* 384:185–188.

77. Cai, P., C. R. Flach, and R. Mendelsohn. 2003. An infrared reflection-absorption spectroscopy study of the secondary structure in (kl4)4k, a therapeutic agent for respiratory distress syndrome, in aqueous monolayers with phospholipids. *Biochemistry.* 42:9446–9452.

78. Martinez-Gil, L., J. Perez-Gil, and I. Mingarro. 2008. The surfactant peptide kl4 sequence is inserted with a transmembrane orientation into the endoplasmic reticulum membrane. *Biophys. J.* 95:L36–L38.

79. Shental-Bechor, D., S. J. Fleishman, and N. Ben-Tal. 2006. Has the code for protein translocation been broken? *Trends Biochem. Sci.* 31:192–196.

80. Dorairaj, S., and T. W. Allen. 2007. On the thermodynamic stability of a charged arginine side chain in a transmembrane helix. *Proc. Natl. Acad. Sci. USA.* 104:4943–4948.

81. Roux, B. 2007. Lonely arginine seeks friendly environment. *J. Gen. Physiol.* 130:233–236.

82. Long, J. R., N. Oyler, G. P. Drobny, and P. S. Stayton. 2002. Assembly of α-helical peptide coatings on hydrophobic surfaces. *J. Am. Chem. Soc.* 124:6297–6303.

83. Degrado, W. F., and J. D. Lear. 1985. Induction of peptide conformation at apolar water interfaces. 1. A study with model peptides of defined hydrophobic periodicity. *J. Am. Chem. Soc.* 107:7684–7689.

84. Strandberg, E., S. Morein, D. T. S. Rijkers, R. M. J. Liskamp, P. C. A. van der Wel, et al. 2002. Lipid dependence of membrane anchoring properties and snorkeling behavior of aromatic and charged residues in transmembrane peptides. *Biochemistry.* 41:7190–7198.

85. Vogt, B., P. Ducarme, S. Schinzel, R. Brasseur, and B. Bechinger. 2000. The topology of lysine-containing amphipathic peptides in bilayers by circular dichroism, solid-state NMR, and molecular modeling. *Biophys. J.* 79:2644–2656.

86. Antharam, V. C., R. S. Farver, A. Kuznetsova, K. H. Sippel, F. D. Mills, et al. 2008. Interactions of the C-terminus of lung surfactant protein B with lipid bilayers are modulated by acyl chain saturation. *Biochim. Biophys. Acta.* 1778:2544–2554.

87. Epand, R. F., R. I. Lehrer, A. Waring, W. Wang, R. Maget-Dana, et al. 2003. Direct comparison of membrane interactions of model peptides composed of only leu and lys residues. *Biopolymers.* 71:2–16.

88. Shai, Y. 1999. Mechanism of the binding, insertion and destabilization of phospholipid bilayer membranes by α-helical antimicrobial and cell non-selective membrane-lytic peptides. *Biochim. Biophys. Acta.* 1462:55–70.

89. Ludtke, S. J., K. He, W. T. Heller, T. A. Harroun, L. Yang, et al. 1996. Membrane pores induced by magainin. *Biochemistry.* 35:13723–13728.

90. Killian, J. A. 1998. Hydrophobic mismatch between proteins and lipids in membranes. *Biochim. Biophys. Acta.* 1376:401–415.

91. Epand, R. M. 1998. Lipid polymorphism and protein-lipid interactions. *Biochim. Biophys. Acta.* 1376:353–368.